Magnetically recyclable Ag/TiO_2 co-decorated magnetic silica composite for photodegradation of dibutyl phthalate with fluorescent lamps

Zhiqiang Ding, Yue Liu, Yong Fu, Feng Chen, Zhangpei Chen and Jianshe Hu

ABSTRACT

In recent years, industrial contaminants and especially organic pollutions have been threatening both environmental safety and human health. Particularly, dibutyl phthalate (DBP) has been considered as one of the major hazardous contaminants due to its widespread production and ecological toxicities. Consequently, reliable methods toward the efficient and environmentally benign degradation of DBP in wastewater would be very desirable. To this end, a novel magnetically separable porous TiO_2/Ag composite photocatalyst with magnetic Fe_3O_4 particles as the core was developed and successfully introduced to the photocatalytic degradation of DBP under visible irradiation with a fluorescent lamp. The presented work describes the grafting of Ag co-doped TiO_2 composite on the silica-modified porous Fe_3O_4 magnetic particles with a simple and inexpensive chemical co-precipitation method. Through the investigation of the influencing factors including photocatalyst dosage, initial concentration of DBP, solution pH, and H_2O_2 content, we found that the degradation efficiency could reach 74%. The photodegradation recovery experiment showed that the degradation efficiency of this photocatalyst remained almost the same after five times of reuse. In addition, a plausible degradation process was also proposed involving the attack of active hydroxyl radicals generated from this photocatalysis system and production of the corresponding intermediates of butyl phthalate, diethyl phthalate, dipropyl phthalate, methyl benzoate, and benzoic acid.

Key words | Ag/TiO_2 co-decorated, dibutyl phthalate, fluorescent lamps, magnetic silica composite, photocatalytic degradation

Zhiqiang Ding
Yue Liu
Yong Fu
Zhangpei Chen (corresponding author)
Jianshe Hu
Center for Molecular Science and Engineering,
College of Science,
Northeastern University,
Shenyang 110819,
China
E-mail: *chenzhangpei@mail.neu.edu.cn*

Feng Chen
Fujian Provincial Key Laboratory of Featured Materials in Biochemical Industry, Fujian Province University Key Laboratory of Green Energy and Environment Catalysis, College of Chemistry and Materials,
Ningde Normal University,
Ningde, Fujian 352100,
China

INTRODUCTION

Industrial contaminants and especially organic pollutions have been threatening both environmental safety and human health, and thus have stimulated extensive research on technological innovation to efficiently remove these contaminants, including by electrochemical method (Sandhwar & Prasad 2017), adsorption method (Wang *et al.* 2016; Yan *et al.* 2016), biodegradation method (Tang *et al.* 2016), photocatalysis (Khataee *et al.* 2009) and other methods (Fang *et al.* 2009). Among them, photocatalytic oxidation has attracted considerable attention in the field of eliminating organic pollutants due to the features of operational convenience, high degradation efficiency in treating organic compounds at low concentrations and relatively low cost (Rajeshwar 2011; O'Shea & Dionysiou 2012). As an important photocatalyst, titanium dioxide (TiO_2) has been widely investigated because of its chemical inertness, long-term stability against corrosion, cost-effectiveness, and being highly photoactive (Legrini *et al.* 1993; Linsebigler *et al.* 1995; Lee *et al.* 2011). Despite much progress having been achieved in the development of photocatalysts composed of hybridized TiO_2, the practical application with these materials still presents great challenges (Hoffmann *et al.* 1995). The separation of these catalyst particles, either at the nano- or microscale, is a major bottleneck because high-energy separation processes are required to prevent the release of such particles into the environment and enable recovery for the reuse of the photocatalysts (Chong *et al.* 2010; Cates 2017). Another barrier is that titania is a wide-bandgap semiconductor and

doi: 10.2166/wst.2020.162

can only absorb about 3–5% of sunlight in the ultraviolet region, which often prevents efficient applications (Carbonaro *et al.* 2013; Nalbandian *et al.* 2015). Therefore, the development of easily recoverable and environmentally friendly light-driven photocatalysts has become a very important topic of research.

During recent decades, phthalate esters (PAEs) have been widely used as excellent plasticizers in the industrial production of various plastics and also employed as indispensable additives in special paints and adhesives (Castle *et al.* 1998). However, phthalates and their related derivatives are toxic and have potential effects on animal and human health (Abdul *et al.* 2017; Hung *et al.* 2017). Recently, under suspicion of being carcinogens and teratogens, PAEs have been classified as top-priority pollutants by the United States Environmental Protection Agency and the European Union (Fang *et al.* 2010). In particular, dibutyl phthalate (DBP) is one of the most widely used PAEs and has been considered as one of the major contaminants due to its high toxicity and bioaccumulation rate (Matsumoto *et al.* 2008). Consequently, the removal of DBP has received increasing attention and some methods have been developed for the treatment of DBP in water or wastewater (Bajt *et al.* 2001; Psillakis *et al.* 2004; Liao *et al.* 2010; Shan *et al.* 2016; Wang *et al.* 2019). Notably, the degradation of DBP under visible light with easily available semiconductors as photocatalysts has gained a lot of interest in recent years. Shan *et al.* (2016) showed that g-C_3N_4/bismuth-based oxide nanocomposites promoted degradation of DBP with up to 60% degradation efficiency under the irradiation of a 500 W halogen tungsten lamp. Recently, a (Bi, Cu) co-doped $SrTiO_3$ nano-composite was fabricated and introduced for the photodegradation of DBP with a metal halide lamp (Jamil *et al.* 2016). Very recently, Akbari-Adergani *et al.* (2018) developed (Fe, Ag) co-doped ZnO nanorods and employed them in the degradation of DBP with a maximum reduction of 95% of DBP at a pH of 3. Despite some progress having been made, it is still challenging work to make practical applications based on these processes owing to the difficulties and high costs of fabrication, recycling and reusing of these particles. Consequently, more efficient and easily recyclable photocatalysts for the degradation of DBP in water would be very desirable.

In previous studies, we successfully fabricated various α-Fe_2O_3 nanoparticles, which exhibited enhanced photocatalytic activity for the degradation of DBP with H_2O_2 under UV light (Liu *et al.* 2018). In this work, to further investigate the efficient degradation of DBP and together with the development of easily recoverable and environmentally friendly light-driven photocatalysts, a new magnetically separable porous TiO_2/Ag composite photocatalyst with magnetic Fe_3O_4 nanoparticles as the core was prepared using tetrabutyl titanate as a titanium source. In addition, magnetic separation is a convenient approach for removing and recycling magnetic particles/composites, and the process has been used for removing heavy metal ions and organic pollutants from water (Gawande *et al.* 2013; Wu *et al.* 2015; Sharma *et al.* 2016). However, to the best of our knowledge, the direct grafting of Ag co-doped TiO_2 nanostructure on porous Fe_3O_4 particles and its structural properties and performance in the photocatalytic degradation of dibutyl phthalate have not been studied so far. This work describes the grafting of Ag co-doped TiO_2 nanostructure on silica-modified porous Fe_3O_4 particles with a simple and inexpensive chemical co-precipitation method for obtaining good photocatalytic degradation of DBP under visible irradiation with a fluorescent lamp. The degradation efficiency could reach 74% and this porous TiO_2/Ag composite photocatalyst could be reused for five runs without a significant loss in efficiency. What is more, the photocatalytic reaction mechanism and degradation process of the DBP were also investigated.

MATERIALS AND METHODS

Chemicals and materials

Butyl titanate, ethyl orthosilicate, silver nitrate, and hydrogen peroxide (30%) were purchased from Tianjin Damao Chemical Co., Ltd (Tianjin, China). Dibutyl phthalate was purchased from Shenyang Licheng Chemical Reagent Plant (Shenyang, China). The α-Fe_2O_3 nanoparticles with different morphologies were prepared according to the processes described in our previous reports (Hu *et al.* 2015). All other solvents and reagents used were purified by standard methods.

Measurements

The morphology of samples was analyzed using a JSM-7800F scanning electron microscope (JEOL, Japan). The absorption wavelength was measured using a UV–Vis spectrophotometer (TU-1901, Beijing Purkinje General Instrument Co., Ltd, China). The degradation products of dibutyl phthalate were analyzed by gas chromatography–mass spectrometry (GC-MS) (HP6890s/HP5973, Perkin-Elmer, Norwalk, USA). The Brunauer–Emmett–Teller (BET) and

Barrett–Joyner–Halenda (BJH) methods were used to determine the surface area and pore-size distribution of the composite materials in N_2 adsorption–desorption (Quadrasorbsi, Quantachrome, USA) experiments at 77 K. Other instruments are listed as follows: thermogravimetric analysis (TGA) was performed with a Diamond instrument, Fourier transform infrared (FT-IR) spectra were measured with samples pressed into KBr pellets on a PerkinElmer Spectrum One (B) spectrometer, and X-ray diffraction (XRD) patterns of samples were detected by a Rigaku DX-2500 X-ray diffractometer.

Synthesis of the magnetic TiO_2/Ag composite photocatalyst

The schematic synthesis of magnetic porous TiO_2/Ag composite photocatalyst (PSCMPs-NH_2-TiO_2/Ag) is shown in Figure 1. The silica-coated Fe_3O_4 magnetic particles (SCMPs) were synthesized according to the previous reported procedure (Vojoudi *et al.* 2017). The α-Fe_3O_4 (0.6 g) and 150 mL of 0.125 mol/L HCl aqueous solution were put into a 500 mL round-bottomed flask, then ultrasound-irradiated for 10 min. The acidified Fe_3O_4 was separated by magnet and washed with deionized water and absolute ethanol until the hydrochloric acid was removed thoroughly. In a 1 L round-bottomed flask, the pretreated Fe_3O_4, 480 mL of ethanol and 120 mL of deionized water were added and stirred vigorously, then 12 mL of aqua ammonia and 1.5 mL of tetraethyl orthosilicate (TEOS) were added and the mixture stirred vigorously for 6 h to obtain the SCMPs.

The obtained SCMPs were dispersed in 240 mL of ethanol, 84 mL of deionized water and 0.06 g CTAB, and then ultrasound-irradiated for 30 min at room temperature. Subsequently, a magnetic bar and 12 mL of TEOS were added, and the mixture was stirred at 80 °C for 12 h. The solid material was collected with a magnet and washed with distilled water and ethanol consecutively. The obtained solid was dispersed in a mixture of 0.72 g ammonium nitrate and 120 mL of ethanol solution, and then refluxed at 80 °C for 24 h to remove the CTAB. The solid was collected with a magnet and washed with distilled water and ethanol, and then dried *in vacuo* to obtain the porous silica-coated Fe_3O_4 magnetic particles (PSCMPs).

The above-obtained PSCMPs were dispersed in 60 mL of ethanol and ultrasound-irradiated for 1 h; 0.6 mL of 3-aminopropyl triethoxysilane (APTES) was added and the mixture was refluxed for 24 h. The naturally cooled reaction mixture was ultrasonically irradiated for 1 h and centrifuged to remove the liquor and afford the corresponding amino functionalized particles (PSCMPs-NH_2). The residue solid PSCMPs-NH_2 was washed with anhydrous ethanol, and then added to 0.16 g $AgNO_3$ and 2 mL of water. The resulted mixture was stirred for 8 h and then 1.5 mL of tetrabutyl titanate and 2 mL of water were added. This mixture was stirred for another 6 h, then poured into a 50 mL beaker and kept stirred until a moist solid formed. Finally, the

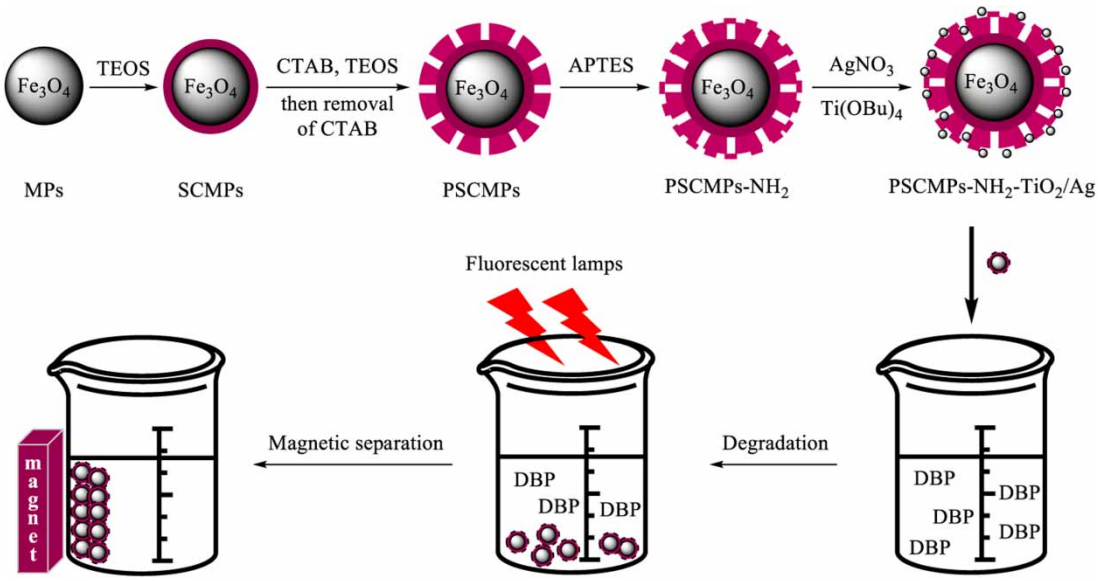

Figure 1 | Preparation of the magnetic photocatalysts and their application for degradation of dibutyl phthalate.

magnetic TiO_2/Ag composite photocatalyst PSCMPs-NH_2-TiO_2/Ag was obtained by drying in an oven at 60–90 °C.

Photodegradation experiments

To explore the effect of the optimum morphology and dosage of the magnetic TiO_2/Ag composite photocatalysts, initial dibutyl phthalate concentration, pH, and H_2O_2 content on the degradation rate of dibutyl phthalate, a batch of photodegradation experiments was conducted. The detailed experimental conditions are shown in Table 1. The experimental operation was performed as follows: 10–30 mg/L of dibutyl phthalate solution (200 mL), 0–500 mg of magnetic TiO_2/Ag composite photocatalyst and 0–60 μL of the 30% H_2O_2 were added into a beaker, and then the pH of the solution was adjusted with dilute HCl or NaOH solution and monitored with a digital pH meter. Then, the mixture was stirred in the dark for 30 min to establish an adsorption–desorption equilibrium between the DBP and the nanocatalysts. Finally, the mixture was placed in the photoreactor and stirred with a magnetic bar (300 rpm) for a certain time at about 25 °C.

As shown in Figure 2, a daylight fluorescent lamp tube (25 W, $\lambda = 400$–750) was used as the light source, the distance between the light source and the top of the reaction mixture was about 15 cm, and the device was cooled by flowing water to ensure that the reaction temperature did not change.

GC-MS experiments

DBP solution (20 mg/L) was placed in the above-mentioned photocatalytic reactor, and then 20 mg composite photocatalyst and 45 μL H_2O_2 were added to the solution for photocatalytic reaction under irradiation with the fluorescent lamp. The reaction liquid was centrifuged and the supernatant was extracted and concentrated before GC-MS analysis. The GC-MS experimental conditions were selected as follows: high-purity He atmosphere was used as carrier gas with flow rate of 2 mL/min, and the tail gas flow was set at 60 mL/min. The column temperature was raised from 100 to 250 °C at a rate of 10 °C/min, and raised to 270 °C at a rate of 3 °C/min. The temperature of the FID detector and the inlet were set at 300 °C and 280 °C, and the sample volume was set to 1 μL with splitless injection.

Table 1 | Degradation conditions

DBP concentration	10–30 mg/L (200 L)
Photocatalyst dosage	0–500 mg
30% H_2O_2 dosage	0–60 μL
pH	5–9
Illumination time	0–3 h

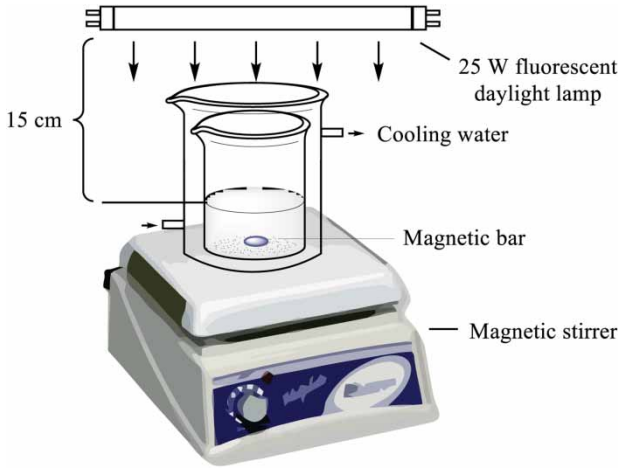

Figure 2 | Reactor of photocatalysis for DBP.

RESULTS AND DISCUSSION

Preparation and characterization of the magnetic photocatalyst

The characterization of the magnetic TiO_2/Ag composite photocatalyst was carried out by FT-IR, XRD, TGA, BET, and scanning electron microscopy (SEM).

Successful functionalization of the PSCMPs-NH_2-TiO_2/Ag can be inferred from FT-IR techniques (Figure 3(a)). The FT-IR spectrum of PSCMPs-NH_2-TiO_2/Ag showed a peak around 567 cm^{-1}, which was attributed to Fe-O vibration resulting from the magnetic Fe_3O_4 core. The peak around the 1,072 cm^{-1} band was caused by the antisymmetric stretching frequency of Si-O-Si, which suggested the silica shells were successfully coated on the magnetic microsphere surface. The peaks at the 3,426 and 1,629 cm^{-1} bands were characteristic of the stretching and bending vibrations of amino groups, meanwhile, absorption bands observed at 2,925 and 2,854 cm^{-1} were attributed to the asymmetrical stretching of alkyl groups, which verified the successful grafting of organic functional groups from APTES onto the surface of SCMPs. According to the IR spectrum of TiO_2, the peak at the 691 cm^{-1} band could be attributed to a Ti-O-Ti vibration, which demonstrated the decoration of TiO_2.

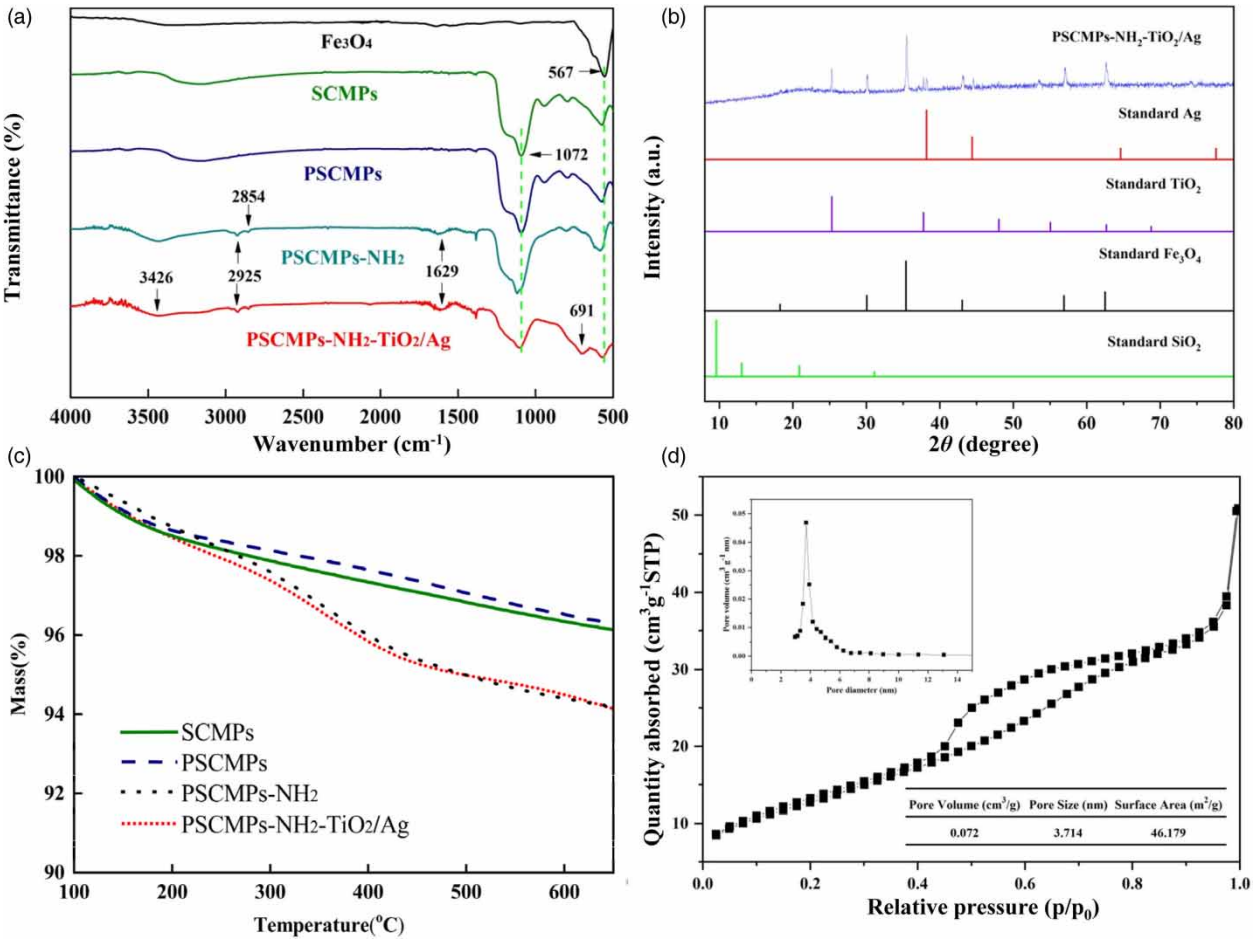

Figure 3 | (a) FT-IR spectra of Fe_3O_4, SCMPs, PSCMPs, PSCMPs-NH_2 and PSCMPs-NH_2-TiO_2/Ag; (b) XRD pattern of PSCMPs-NH_2-TiO_2/Ag; (c) TGA curves of SCMPs, PSCMPs, PSCMPs-NH_2 and PSCMPs-NH_2-TiO_2/Ag; (d) N_2 adsorption–desorption isotherms and pore-size distribution of PSCMPs-NH_2-TiO_2/Ag.

Figure 3(b) shows the XRD patterns of PSCMPs-NH_2-TiO_2/Ag, JCPDS file of Fe_3O_4 (PDF#72-2303), SiO_2 (PDF#89-0735), TiO_2 (PDF#71-11665) and Ag (PDF#65-8428). The position and relative intensities of peaks in the XRD pattern of PSCMPs-NH_2-TiO_2/Ag conform well with the standard XRD pattern of Fe_3O_4, indicating retention of the crystalline cubic spinel structure during the silicon-covering, amino-functionalized and grafting Ag co-doped TiO_2 processes. Diffraction peaks located at $2\theta = 25.23°$, 37.94°, 48.01°, 54.64° and 62.69° were in accordance with the standard data of anatase-type titanium dioxide. Diffraction peaks located at $2\theta = 38.2°$ and 44.6° were in accordance with the standard data of Ag. In addition, compared with standard XRD patterns of SiO_2, no high-intensity peaks of SiO_2 were observed. Together with the literature report (Zhou *et al.* 2017), we conceived that the coated silica belonged to amorphous silica.

The TGA was used to determine the percentage of organic functional groups chemisorbed onto the surface of the magnetic particles (Figure 3(c)). The TGA curve of the PSCMPs-NH_2-TiO_2/Ag shows a first degradation stage below 150 °C, and this may have resulted from the loss of physically adsorbed and chemisorbed water or solvent on the surface of the samples (Yu *et al.* 2012). The second degradation stage with a weight loss of about 3% from 150 to 600 °C was ascribed to decomposition of organic materials grafting to the PSCMPs-NH_2-TiO_2/Ag particles.

Textural characteristics of PSCMPs-NH_2-TiO_2/Ag including the total pore volumes (Vtotal, $cm^3 \cdot g^{-1}$), the pore size (DBJH, nm) and the BET surface area (SBET, $m^2 \cdot g^{-1}$) were measured with N_2 physisorption techniques at 77 K (Figure 3(d)). Notably, the isotherms of PSCMPs-NH_2-TiO_2/Ag belonged to the characteristic type IV classification, indicating that this class of NPs exerted a mesoporous structure. By employing the Barrett–Joyner–Halenda model,

at the stage of $0 < P/P_0 < 0.4$, due to the monolayer adsorption, the adsorption amount at this time increased linearly with the partial pressure. When $0.4 < P/P_0 < 0.8$, a hysteresis loop appears in the isotherms, and the pore size distribution diagram shows a unimodal distribution. Therefore, we can infer that PSCMPs-NH_2-TiO_2/Ag belonged to a mesoporous structure with an average pore diameter of 3.714 nm, a pore volume of 0.072 cm^3/g, and surface area of 46.179 m^2/g.

The SEM images of the synthesized NPs are shown in Figure 4. Figure 4(a) shows that Fe_3O_4 nanoparticles are spherical in shape with an average size of about 150 nm. Compared with Fe_3O_4, the surfaces of SCMPs and PSCMPs-NH_2 were still spherical and of nearly uniform size except appearing to have a slight aggregation. The SEM image of PSCMPs-NH_2-TiO_2/Ag demonstrates an interconnection of the nearly spherical particles with size in the range of 100–150 nm.

Establishment of the standard curve

A series of standard DBP solutions (10, 15, 20, 25 and 30 mg/L) were scanned at 210–400 nm by UV–Vis spectrophotometer; the characteristic absorption wavelength was 230 nm and the results are provided in Figure 5. From Figure 5(b) we can infer that the DBP concentration in the measurement range was linear with the absorbance of the solution and the regression equation could be obtained as $A = 0.02c + 0.008$ (where A represents absorbance, c represents the DBP concentration). What is more, the degradation efficiency could be calculated according to the following equation:

$$K = \frac{A_0 - A_t}{A_0} \times 100\%$$

where K is the efficiency, and A_0 and A_t represent the absorbance of the initial solution and the solution at time t, respectively.

Effects of degradation conditions on degradation efficiency

Kaneco *et al.* (2006) have investigated the operational parameters including initial DBP concentration, H_2O_2 dosage, TiO_2/Ag composite dosage and pH of the degradation solvent, which play critical roles in the photodegradation process and thus affect the photodegradation efficiency. Therefore, the effects of these parameters were evaluated in the next investigation and the results are summarized in Figure 6.

The effect of initial DBP concentration on the degradation rate is depicted in Figure 6(a). Notably, the degradation rate of DBP increased first and then decreased

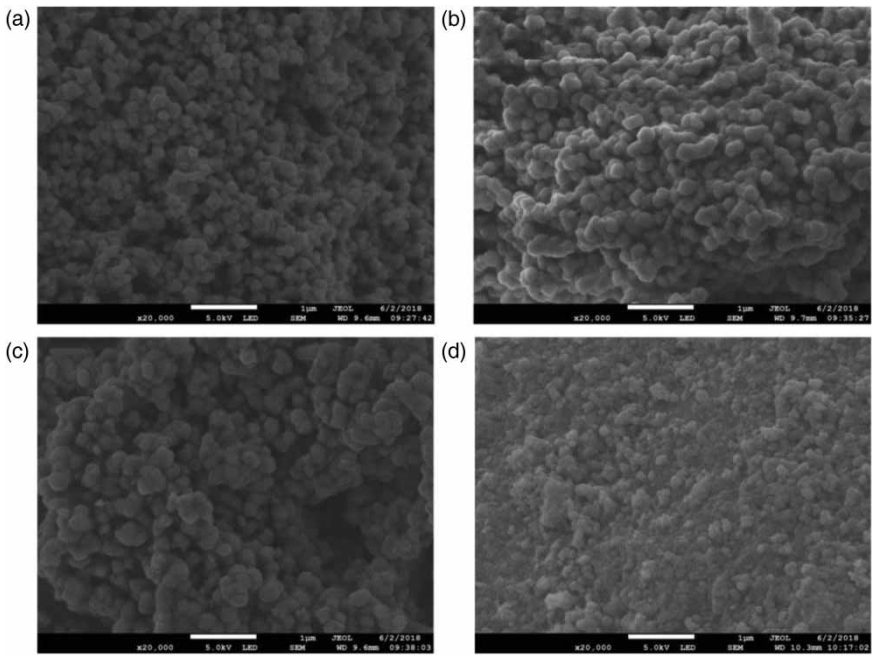

Figure 4 | SEM images of (a) MPs, (b) SCMPs, (c) PSCMPs-NH_2, (d) PSCMPs-NH_2-TiO_2/Ag.

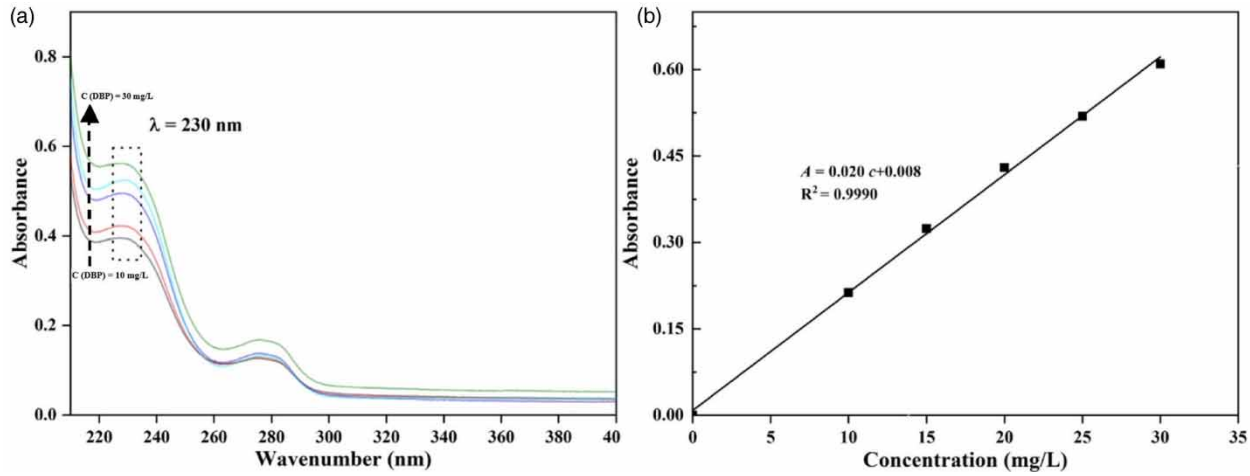

Figure 5 | (a) Ultraviolet absorption spectrum of DBP solutions; (b) relationship between concentration and absorbance of DBP solution at 230 nm.

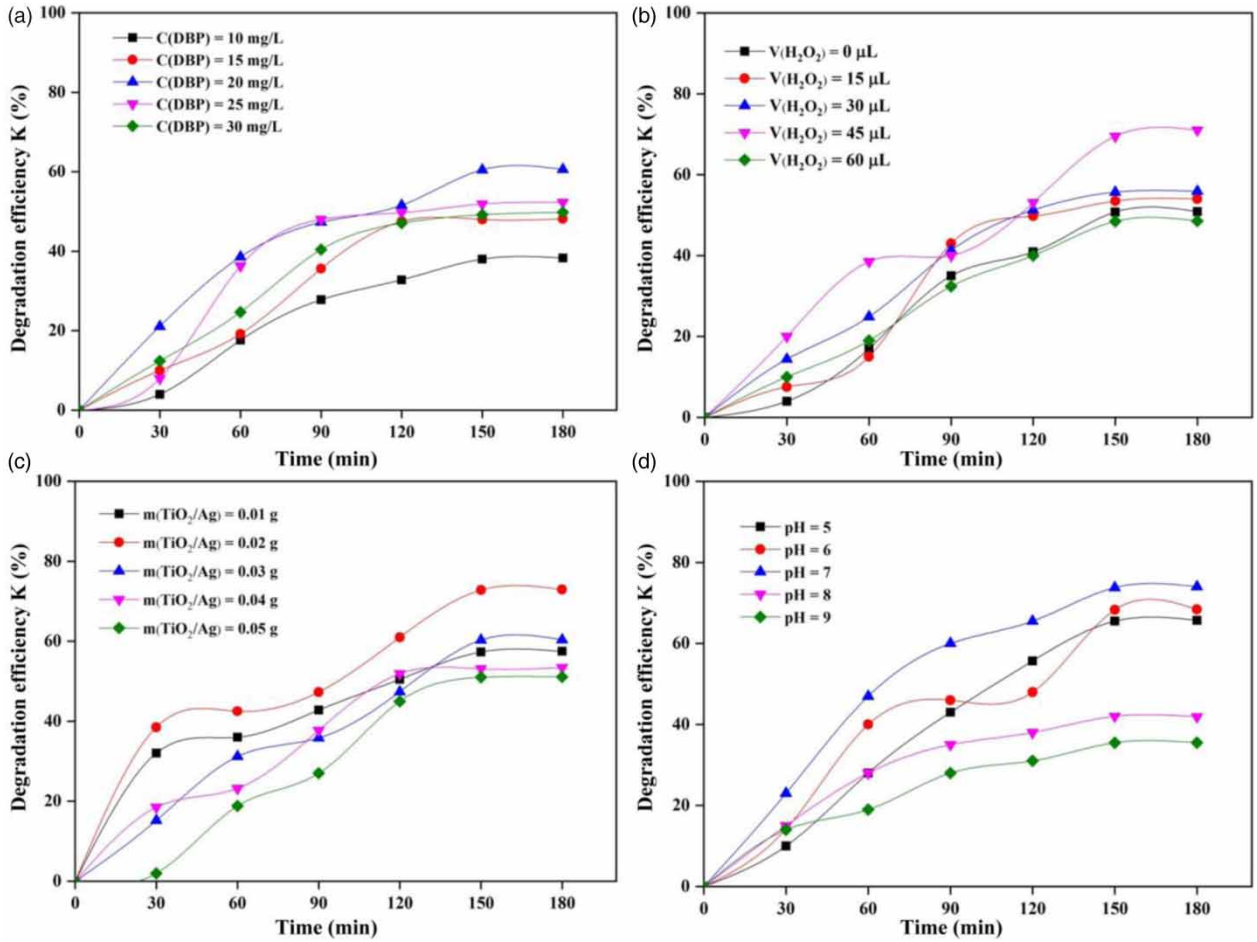

Figure 6 | (a) Effects of initial DBP concentration; (b) effects of H_2O_2 dosage; (c) effects of photocatalyst dosage; (d) effects of pH on DBP degradation efficiency.

with the increase of initial concentration. When the initial concentration of the solution was 20 mg/L, the highest degradation rate of DBP was achieved and the maximum degradation rate was 61%. Therefore, 20 mg/L of DBP solution was selected as the initial DBP concentration for degradation in the further investigation.

The H_2O_2 dosage also plays a critical role in the photodegradation process because the photolysis of H_2O_2 could generate reactive hydroxyl radicals under light irradiation to facilitate the degradation. As shown in Figure 6(b), the degradation rate tended to firstly increase and then decrease with the increase of the H_2O_2 dosage. When the dosage of the 30% H_2O_2 was 45 μL, the photocatalytic degradation rate of DBP was the highest. With continued increase of H_2O_2 dosage, the degradation rate decreased. Possible reasons are described as follows: the H_2O_2 had a certain ability to capture •OH and generated the less active radical species HO_2• and inhibited the degradation of DBP (Vidal *et al.* 2015). When the dosage of the 30% H_2O_2 increased to more than 45 μL, the inhibition effect became more obvious. Consequently, the H_2O_2 dosage was selected as 45 μL in the next study.

The catalyst dosage is also an important parameter in suspended degradation processes, so it is necessary to explore the effect of the catalyst dosage on the degradation efficiency of DBP (Figure 6(c)). To determine the optimal dosage, various amounts of the catalyst was tested. Five 200 mL of 20 mg/L DBP solutions were added with 0.01, 0.02, 0.03, 0.04 and 0.05 g magnetic titanium dioxide/Ag composite photocatalysts, respectively. The absorbance was measured every ten minutes in a dark room. Then 45 μL of 30% H_2O_2 was added and the absorbance of this mixture was measured every 30 minutes under irradiation with a fluorescent lamp. When the composite photocatalyst dosage increased from 0.01 to 0.02 g, the DBP degradation increased from 60.4% to 72.9%. This might be ascribed to the amount of photo-generated electron–hole and hydroxyl radicals increasing when the active sites of the photocatalytic reaction increased. However, the degradation efficiency decreased when the dosage of magnetic titanium dioxide/Ag increased to 0.03 g or more. This may be caused by the excess amount of the photocatalyst reducing light penetration and leading to a decrease of the photo-generated electron–hole pairs.

The pH of the solution is an important factor affecting the degradation process for the following reasons: (1) H^+ or OH^- in the solution can change the electron properties of photocatalysts, which will affect the adsorption behavior of organic molecules on the surface of catalysts; (2) the solution pH can affect the decomposition rate of H_2O_2 and consequently affect the degradation rate; and (3) different pH can also lead to structural changes of some organic compounds, which will change the process of catalytic degradation. Figure 6(d) shows the degradation efficiency with irradiation time in the pH range of 5–9. The results demonstrated that the highest degradation efficiency could be achieved under neutral conditions and the degradation rate decreased under acidic or alkaline conditions, especially in alkaline solution. Under alkaline conditions, H_2O_2 was unstable and easily decomposed into H_2O and O_2, and this affected the generation of •OH, and made the photocatalytic degradation rate decrease. In acidic and neutral conditions, hydrogen peroxide was relatively stable, but the generated organic acids (such as benzoic acid, carboxylic acid) and CO_2 might suppress the degradation process. In this regard, a solution pH of 7 was suggested for DBP degradation, and the degradation rate reached 74%.

The recycling experiment of photodegradation

The photocatalytic efficiency of the PSCMPs-NH_2-TiO_2/Ag nanoparticles for multiple usages was investigated in the next investigation and the results are shown in Figure 7. Due to the possessing of a magnetic Fe_3O_4 core, the obtained NPs could be separated conveniently with an external magnetic bar after the photocatalytic degradation process, and could be reused directly for the photodegradation of fresh DBP solution. After five cycles of reuse, the degradation performance of PSCMPs-NH_2-TiO_2/Ag still remained with 70% efficiency.

Photocatalytic degradation reaction mechanism

The corresponding degradation intermediates of DBP were analyzed by GC-MS. We detected degradation intermediates including butyl phthalate, diethyl phthalate, dipropyl

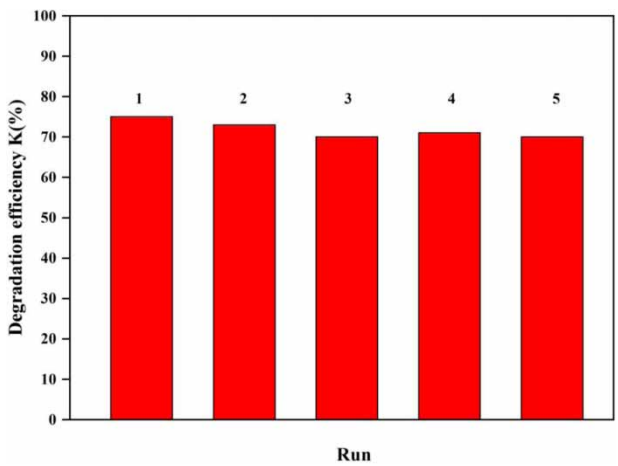

Figure 7 | Reusability of the catalyst.

phthalate, methyl benzoate, and benzoic acid. The corresponding retention times were 14.965, 11.398, 11.122 and 8.566 min, respectively. Based on the results, the probable photocatalytic degradation pathway of DBP was proposed and is depicted in Figure 8. In the reaction, the modified titanium dioxide photocatalyst generated the electron–hole pairs when stimulated by light. Then the generated electron–hole pairs were transferred to the surface of the catalyst and combined with OH^-, O_2, H_2O, etc. along with the exchange of energy and charge to form hydroxyl radicals •OH with strong oxidizability. Subsequently, the attack of hydroxyl radicals on DBP led to two possible processes. The first is that the C-O bond of the DBP was broken down and formed monobutyl phthalate followed by the breaking down of another C-O bond to generate phthalic acid. The further degradation of phthalic acid produced benzoic acid which was degraded to CO_2 and H_2O according to previous reports (Liu *et al.* 2018). The second way is that some DBP molecules started to degrade from the carbon chain at different locations and the main products such as dipropyl phthalate and diethyl phthalate appeared. With the continuous action of •OH, methyl benzoate and benzoic acid were generated in the next steps. Similarly, the benzoic acid was eventually oxidized to CO_2 and H_2O by the active hydroxyl radicals.

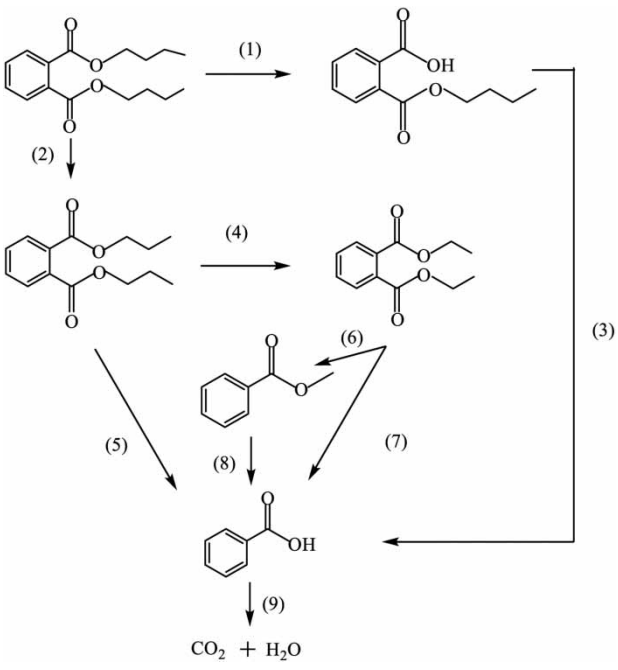

Figure 8 | Proposed photocatalytic degradation pathways of DBP.

CONCLUSIONS

A novel magnetically separable porous TiO_2/Ag composite photocatalyst with magnetic Fe_3O_4 nanoparticles as the core was developed and successfully introduced to the photocatalytic degradation of DBP under visible irradiation with a fluorescent lamp. A degradation efficiency of 74% was achieved with 0.02 g of photocatalyst in 200 mL of DBP (20 mg/L) solution under the conditions of pH = 7 and 45 μL of H_2O_2 dosage. The DBP could be degraded by the attack of active hydroxyl radicals produced from this environmentally friendly light-driven photocatalysis system, and the corresponding intermediates were butyl phthalate, diethyl phthalate, dipropyl phthalate, methyl benzoate, and benzoic acid, which could be further oxidized to CO_2 and H_2O. These results illustrated that this magnetically separable porous TiO_2/Ag composite material has great potential as a catalyst to eliminate toxic organic pollutants in the environment and provides a means for photocatalytic degradation of organic toxicants.

ACKNOWLEDGEMENTS

This work was supported by the Science and Technology Foundation of Liaoning Province (20170520185), and Fundamental Research Funds for the Central Universities (N180506002, N180705004).

REFERENCES

Abdul, G., Zhu, X.-Y. & Chen, B.-L. 2017 Structural characteristics of biochar–graphene nanosheet composites and their adsorption performance for phthalic acid esters. *Chem. Eng. J.* **319**, 9–20.

Akbari-Adergani, B., Saghi, M. H., Eslami, A., Mohseni-Bandpei, A. & Rabbani, M. 2018 Removal of dibutyl phthalate from aqueous environments using a nanophotocatalytic Fe, Ag-ZnO/VIS-LED system: modeling and optimization. *Environ. Technol.* **39** (12), 1566–1576.

Bajt, O., Mailhot, G. & Bolte, M. 2001 Degradation of dibutyl phthalate by homogeneous photocatalysis with Fe(III) in aqueous solution. *Appl. Catal. B* **33**, 239–248.

Carbonaro, S., Sugihara, M. N. & Strathmann, T. J. 2013 Continuous-flow photocatalytic treatment of pharmaceutical micropollutants: activity, inhibition, and deactivation of TiO_2 photocatalysts in wastewater effluent. *Appl. Catal. B.* **129**, 1–12.

Castle, L., Mercer, A. J., Startin, J. R. & Gilbert, J. 1998 Migration from plasticized films into foods 3. Migration of phthalate,

sebacate, citrate and phosphate esters from films used for retail food packaging. *Food Addit. Contam.* **5**, 9–20.

Cates, E. L. 2017 Photocatalytic water treatment: so where are we going with this? *Environ. Sci. Technol.* **51**, 757–758.

Chong, M.-N., Jin, B., Chow, C. W. K. & Saint, C. 2010 Recent developments in photocatalytic water treatment technology: a review. *Water Res.* **44**, 2997–3027.

Fang, C., Long, Y., Wang, W., Feng, H. & Shen, D. 2009 Behavior of dibutyl phthalate in a simulated landfill bioreactor. *J. Hazard Mater.* **167**, 86–192.

Fang, C.-R., Yao, J., Zheng, Y.-G., Jiang, C.-J., Hu, L.-F., Wu, Y.-Y. & Shen, D.-S. 2010 Dibutyl phthalate degradation by *Enterobacter* sp. T5 isolated from municipal solid waste in landfill bioreactor. *Int. Biodeterior. Biodegrad* **64**, 442–446.

Gawande, M. B., Branco, P. S. & Varma, R. S. 2013 Nano-magnetite (Fe_3O_4) as a support for recyclable catalysts in the development of sustainable methodologies. *Chem. Soc. Rev.* **42**, 3371–3393.

Hoffmann, M. R., Martin, S. T., Choi, W. & Bahnemann, D. W. 1995 Environmental applications of semiconductor photocatalysis. *Chem. Rev.* **95**, 69–96.

Hu, J.-S., Sun, N., Li, S. & Qin, G.-W. 2015 Controllable preparation of α-Fe_2O_3 particles with different morphology. *J. Northeast. Univ.* **36**, 1260–1264.

Hung, C.-H., Yuan, C. & Li, H.-W. 2017 Photodegradation of diethyl phthalate with PANi/CNT/TiO_2 immobilized on glass plate irradiated with visible light and simulated sunlight – effect of synthesized method and pH. *J. Hazard. Mater.* **322**, 243–253.

Jamil, T. S., Abbas, H. A., Youssief, A. M., Mansor, E. S. & Hammad, F. F. 2016 The synthesis of nano-sized undoped, Bi doped and Bi, Cu co-doped $SrTiO_3$ using two sol–gel methods to enhance the photocatalytic performance for the degradation of dibutyl phthalate under visible light. *C. R. Chim.* **20**, 97–106.

Kaneco, S., Katsumata, H., Suzuki, T. & Ohta, K. 2006 Titanium dioxide mediated photocatalytic degradation of dibutyl phthalate in aqueous solution – kinetics, mineralization and reaction mechanism. *Chem. Eng. J.* **125**, 59–66.

Khataee, A. R., Pons, M. N. & Zahraa, O. 2009 Photocatalytic degradation of three azo dyes using immobilized TiO_2 nanoparticles on glass plates activated by UV light irradiation: influence of dye molecular structure. *J. Hazard. Mater.* **168**, 451–457.

Lee, J., Kim, J. & Choi, W. 2011 TiO_2 photocatalysis for the redox conversion of aquatic pollutants. In: *Aquatic Redox Chemistry* (P. G. Tratnyek, T. J. Grundl & S. B. Haderlein, eds). ACS Symposium Series Vol. 1071, American Chemical Society, Washington, DC, USA, pp. 199–222.

Legrini, O., Oliveros, E. & Braun, A. M. 1993 Photochemical processes for water treatment. *Chem. Rev.* **93**, 671–698.

Liao, C., Chen, L., Chen, B. & Lin, S. 2010 Bioremediation of endocrine disruptor di-*n*-butyl phthalate ester by *Deinococcus radiodurans* and *Pseudomonas stutzeri*. *Chemosphere* **78**, 342–346.

Linsebigler, A. L., Lu, G. & Yates, J. T. 1995 Photocatalysis on TiO_2 surfaces: principles, mechanisms, and selected results. *Chem. Rev.* **95**, 735–758.

Liu, Y., Sun, N., Hu, J., Li, S. & Qin, G. 2018 Photocatalytic degradation properties of α-Fe_2O_3 nanoparticles for dibutyl phthalate in aqueous solution system. *Roy. Soc. Open Sci.* **5**, 172196.

Matsumoto, M., Hirata-Koizumi, M. & Ema, M. 2008 Potential adverse effects of phthalic acid esters on human health: a review of recent studies on reproduction. *Regul. Toxicol. Pharm.* **50**, 37–49.

Nalbandian, M. J., Greenstein, K. E., Shuai, D., Zhang, M., Choa, Y. H., Parkin, G. F., Myung, N. V. & Cwiertny, D. M. 2015 Tailored synthesis of photoactive TiO_2 nanofibers and Au/TiO_2 nanofiber composites: structure and reactivity optimization for water treatment applications. *Environ. Sci. Technol.* **49**, 1654–1663.

O'Shea, K. E. & Dionysiou, D. D. 2012 Advanced oxidation processes for water treatment. *J. Phys. Chem. Lett.* **3**, 2112–2113.

Psillakis, E., Mantzavinos, D. & Kalogerakis, N. 2004 Monitoring the sonochemical degradation of phthalate esters in water using solid-phase microextraction. *Chemosphere* **54**, 849–857.

Rajeshwar, K. 2011 Solar energy conversion and environmental remediation using inorganic semiconductor–liquid interfaces: the road traveled and the way forward. *J. Phys. Chem. Lett.* **2**, 1301–1309.

Sandhwar, V. K. & Prasad, B. 2017 Comparative study of electrochemical oxidation and electrochemical Fenton processes for simultaneous degradation of phthalic and para-toluic acids from aqueous medium. *J. Mol. Liq.* **243**, 519–532.

Shan, W., Hu, Y., Bai, Z., Zheng, M. & Wei, C. 2016 In situ preparation of g-C_3N_4/bismuth-based oxide nanocomposites with enhanced photocatalytic activity. *Appl. Catal. B* **188**, 1–12.

Sharma, R. K., Dutta, S., Sharma, S., Zboril, R., Varma, R. S. & Gawande, M. B. 2016 Fe_3O_4 (iron oxide)-supported nanocatalysts: synthesis, characterization and applications in coupling reactions. *Green Chem.* **18**, 3184–3209.

Tang, W.-J., Zhang, L.-S., Fang, Y., Zhou, Y. & Ye, B.-C. 2016 Biodegradation of phthalate esters by newly isolated *Rhizobium* sp. LMB-1 and its biochemical pathway of di-*n*-butyl phthalate. *J. Appl. Microbiol.* **121**, 177–186.

Vidal, E., Negro, A., Cassano, A. & Zalazar, C. 2015 Simplified reaction kinetics, models and experiments for glyphosate degradation in water by the UV/H_2O_2 process. *Photochem. Photobiol. Sci.* **14**, 366–377.

Vojoudi, H., Badiei, A., Bahar, S., Ziarani, G. M., Faridbod, F. & Ganjali, M. R. 2017 A new nano-sorbent for fast and efficient removal of heavy metals from aqueous solutions based on modification of magnetic mesoporous silica nanospheres. *J. Mag. Mag. Mater.* **441**, 93–203.

Wang, J.-L., Lou, Y.-Y., Xu, C., Song, S. & Liu, W.-P. 2016 Magnetic lanthanide oxide catalysts: an application and comparison in

the heterogeneous catalytic ozonation of diethyl phthalate in aqueous solution. *Sep. Purif. Technol.* **159**, 57–67.

Wang, G., Zhang, Q., Chen, Q., Ma, X., Xin, Y., Zhu, X., Ma, D., Cui, C., Zhang, J. & Xiao, Z. 2019 Photocatalytic degradation performance and mechanism of dibutyl phthalate by graphene/TiO_2 nanotube array photoelectrodes. *Chem. Eng. J.* **358**, 1083–1090.

Wu, W., Jiang, C. & Roy, V. A. L. 2015 Recent progress in magnetic iron oxide–semiconductor composite nanomaterials as promising photocatalysts. *Nanoscale* **7**, 38–58.

Yan, X.-L., Yang, Y.-L., Wang, C., Hu, X.-Y., Zhou, M. & Komarneni, S. 2016 Surfactant-assisted synthesis of ZIF-8 nanocrystals for phthalic acid adsorption. *J. Sol-Gel. Sci. Technol.* **80**, 523–530.

Yu, Y., Addai-Mensah, J. & Losic, D. 2012 Functionalized diatom silica microparticles for removal of mercury ions. *Sci. Technol. Adv. Mater.* **13**, 015008.

Zhou, J.-J., Li, Y.-N., Sun, H.-B., Tang, Z.-K., Qi, L., Liu, L., Ai, Y.-J., Li, S., Shao, Z.-X. & Liang, Q.-L. 2017 Porous silica-encapsulated and magnetically recoverable Rh NPs: a highly efficient, stable and green catalyst for catalytic transfer hydrogenation with 'slow-release' of stoichiometric hydrazine in water. *Green Chem.* **19**, 3400–3407.

First received 29 August 2019; accepted in revised form 27 March 2020. Available online 7 April 2020